

**Precision Feshbach spectroscopy of ultracold Cs<sub>2</sub>**Cheng Chin,<sup>\*</sup> Vladan Vuletić,<sup>†</sup> Andrew J. Kerman,<sup>‡</sup> and Steven Chu<sup>‡</sup>  
*Department of Physics, Stanford University, Stanford, California 94305-4060, USA*Eite Tiesinga, Paul J. Leo,<sup>§</sup> and Carl J. Williams  
*Atomic Physics Division, National Institute of Standards and Technology, Gaithersburg, Maryland 20899-8423, USA*  
(Received 24 December 2003; published 3 September 2004)

We have observed and located more than 60 magnetic field-induced Feshbach resonances in ultracold collisions of ground-state <sup>133</sup>Cs atoms. Multiple extremely weak Feshbach resonances associated with *g*-wave molecular states are detected through variations in the radiative collision cross sections. The Feshbach spectroscopy allows us to determine the interactions between ultracold cesium atoms and the molecular energy structure near the dissociation continuum with unprecedented precision. Our work not only represents a very successful collaboration of experimental and theoretical efforts, but also provides essential information for cesium Bose-Einstein condensation, Cs<sub>2</sub> molecules, and atomic clock experiments.

DOI: 10.1103/PhysRevA.70.032701

PACS number(s): 34.50.-s, 05.30.Jp, 32.80.Pj, 67.40.Hf

**I. INTRODUCTION**

The collision properties of an ultracold and dilute atom gas are strongly influenced by the long-range interactions between two atoms. When the interaction potential supports a weakly bound state near the scattering energy, the atomic collision properties can be resonantly altered, a situation referred to as a Feshbach resonance [1,2]. In many cold-atom systems, magnetically tunable Feshbach resonances have been discovered and have led to ground-breaking observations including the implosion of a Bose-Einstein condensate (BEC) [3], the coherent coupling between an atomic BEC and molecules [4], the creation of bright solitons [5], and recently the creation of ultracold molecules [6–8] and of a molecular BEC [9].

The collisional properties of ultracold cesium atoms have intrigued experimentalists and theorists because of their large clock shifts [10], enormous collision cross sections [11], and the extreme difficulty to reach BEC [12]. These anomalies in the atom-atom scattering can be explained by the coupling of the scattering continuum to molecular states. While these states cannot be accessed by conventional spectroscopy [13], they may be tuned into resonance with the scattering continuum and induce Feshbach resonances. Detection of multiple Feshbach resonances, or Feshbach spectroscopy, permits a precise determination of the long-range interaction parameters, as well as the molecular structure near threshold. With this information, the cold collision anomalies can be resolved and the clock shifts [14], collision cross sections

and scattering lengths can be accurately calculated [15].

In this work, we report the observation of more than 60 Feshbach resonances of cesium atoms in 10 different incident channels. In particular, we employ a radiative detection scheme to resolve narrow resonances [6,16] whose locations allow us to significantly improve our determination of Cs interaction parameters over our previous work [15,17]. With these parameters, the molecular energy structure near threshold as well as *s*-wave scattering lengths and collision properties can be precisely determined.

We organize the paper as follows. First, we outline the experimental setup and procedures and the general measurement methods in Sec. II. We present and discuss the results from inelastic Feshbach spectroscopy, elastic Feshbach spectroscopy, and radiative spectroscopy in Secs. III–V, respectively. In Sec. VI we discuss the Hamiltonian for two ground-state cesium atoms and approximate quantum numbers for the system. The numerical procedures for calculating scattering properties and bound-state energies are presented in Sec. VII. Section VIII analyzes all observed Feshbach resonances and assigns quantum numbers to each resonance.

**II. EXPERIMENT****A. Feshbach spectroscopy**

Feshbach resonance in binary atomic collisions is illustrated in Fig. 1. Interacting atom pairs in the scattering continuum, or scattering channel, couple to a discrete bound state supported by a closed channel with higher internal energy. This coupling resonantly alters the outgoing scattering amplitude in the scattering channel (elastic collision resonance) and in the lower-lying open channels (inelastic collision resonance).

In ultracold-atom experiments, Feshbach resonances can be observed in elastic and inelastic collision rates [2,18] and in the molecular population, probed by photoassociation [19] or photodissociation [6] as shown in Fig. 1.

In most cases the magnetic moments of the molecular state and the scattering continuum are unequal, such that the

<sup>\*</sup>Present address: Institut für Experimentalphysik, Universität Innsbruck, Technikerstr. 25, 6020 Innsbruck, Austria.

<sup>†</sup>Present address: MIT-Harvard Center for Ultracold Atoms, Massachusetts Institute of Technology, Cambridge, MA 02139, USA.

<sup>‡</sup>Present address: Lawrence Berkeley National Laboratory, One Cyclotron Road, Mail Stop 50A-4112, Berkeley, CA 94720, USA.

<sup>§</sup>Present address: National Human Genome Research Institute, 49 Convent Drive, Bldg 49, Bethesda, MD 20874-4472, USA.

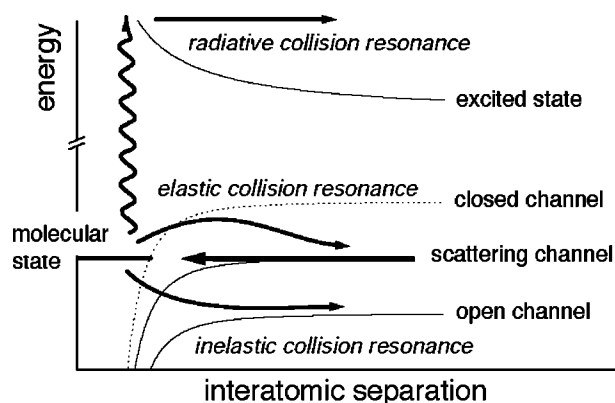


FIG. 1. Illustration of radiative, elastic, and inelastic Feshbach resonance. The molecular state is supported by the closed channel.

energy difference between the molecular state and the colliding atom pair can be tuned by means of an external magnetic field. The molecular bound-state energy structure near the dissociation threshold is then reflected in the magnetic field dependence of the atom-atom scattering. A measurement of the ultracold collision properties as a function of magnetic field (Feshbach spectrum) in combination with theoretical modeling thus unveils the underlying molecular spectrum. In this work, we are able to associate each resonance with its quantum numbers of both the incoming scattering channel and the molecular state, where it is noteworthy that the  $s$ ,  $p$ ,  $d$ , ... partial waves of the incoming channel and of the resonance need not be the same. A collection of Feshbach spectra for colliding atoms in several different quantum states then provides the information necessary to accurately determine the long-range interaction parameters and the molecular energy structure near the dissociation continuum.

### B. Preparation of ultracold high-density samples

In order to measure Feshbach spectra with good signal-to-noise ratio and high resolution and to simplify the theoretical analysis, it is favorable to use high-density samples of ultracold atoms confined in a trap that produces negligible tensor light shifts of the atomic and molecular energy levels [20]. We use a far-detuned, linearly polarized, one-dimensional (1D) optical lattice trap to confine the atoms, in conjunction with an optical cooling method that can produce high-density samples at  $\mu\text{K}$  temperatures [21,22].

Figure 2 shows schematically the experimental setup. Ultracold samples of cesium atoms are prepared in the upper part of a compact ultrahigh-vacuum chamber. A pair of magnetic field coils, when operated in the anti-Helmholtz configuration with opposite currents, provides the spherical quadrupole field for a magneto-optical trap (MOT) and, in the Helmholtz configuration, produces a homogeneous magnetic field up to 25 mT. A linearly polarized, vertically propagating, retroreflected Nd:YAG laser beam provides the far-detuned one-dimensional lattice dipole trap at 1064 nm [21]. The number of trapped atoms is inferred from the fluorescence emitted by the cloud when it is illuminated with resonant light on the  $F_g=4 \rightarrow F_e=5$  hyperfine component of

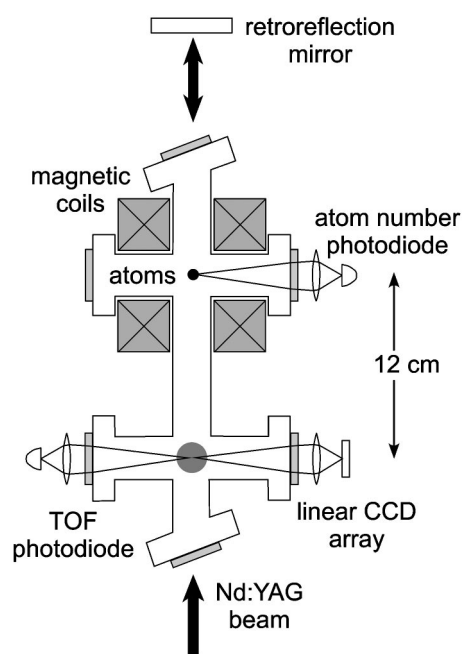


FIG. 2. Apparatus for Feshbach spectroscopy of  $^{133}\text{Cs}$ .

the  $D_2$  line near 852 nm. Cloud temperatures in the vertical and horizontal directions are determined by releasing the atoms and performing time-of-flight imaging 12 cm below onto a photodiode and a linear charge-coupled-device (CCD) array, respectively. Trap vibration frequencies are measured by parametric excitation [23]. The atomic density is derived from the measured atom number, temperature, and trap vibration frequencies, as detailed in Ref. [17].

The ultracold sample is prepared by first collecting  $5 \times 10^8$  atoms in a vapor-cell MOT in 500 ms. Superimposed with the MOT is the YAG 1D optical lattice dipole trap that at a power of 8 W and a beam waist of  $260 \mu\text{m}$  provides a trap depth of  $U/h=1.6$  MHz and axial and radial vibration frequencies of  $\omega_a/2\pi=50$  kHz and  $\omega_r/2\pi=80$  Hz, respectively. The preparation of the high-density sample in the YAG dipole trap is accomplished by means of two phases of Raman-sideband cooling (RSC) with a 3D near-detuned optical lattice [22]. We extinguish the MOT light and apply the first RSC for 10 ms in a small bias field of  $5 \mu\text{T}$ , which cools the atoms to temperatures below  $1 \mu\text{K}$  and predominantly polarizes them into the lowest-energy magnetic sublevel  $|6S_{1/2}, F=3, m_F=3\rangle$ . Here  $F$  is the total angular momentum of cesium atoms in the  $6S_{1/2}$  ground state and  $m_F$  is the angular momentum projection along the magnetic field direction. When the 3D near-detuned optical lattice is extinguished in 1 ms, the release of the atoms into the 1D YAG lattice trap is adiabatic only in the vertical direction, and we observe a radial oscillation as the atoms slide down the trap potential. To remove some of the excess potential energy, we wait for 4 ms until the atoms have the greatest kinetic energy and highest density, and perform a second phase of RSC [24]. Due to the high density near  $10^{12} \text{cm}^{-3}$ , the second cooling requires a weaker optical pumping intensity and longer cooling time of 15 ms. After rethermalization for 200 ms in the YAG lattice trap,  $1 \times 10^8$  atoms are prepared at a temperature of  $3\text{--}5 \mu\text{K}$  with a vertical (horizontal) rms

radius of  $\sigma_z=580 \mu\text{m}$  ( $\sigma_x=30 \mu\text{m}$ ). This means that near the central region, each site in the 1D YAG lattice trap contains  $4 \times 10^4$  atoms at a mean density of approximately  $1 \times 10^{13} \text{cm}^{-3}$ . The two phases of RSC also allow us to adjust almost independently the atomic density and temperature by changing the detuning of the optical pumping beam during the first and second RSC phases, respectively.

The preparation of pure samples in desired target states is crucial for cold collision experiments because different internal states can have drastically different collision properties. To improve the atomic polarization over that achieved by the RSC alone, we apply an additional optical pumping pulse for 3 ms during the release from the second RSC phase. This has the advantage that atom-atom collisions are still suppressed due to the 3D confinement in the near-detuned optical lattice, which prevents radiative collision loss. Using microwave spectroscopy, we optimize the optical pumping process at a bias field of  $14 \mu\text{T}$  and prepare up to 98% of the atoms in one of the stretched states  $|F, m_F=\pm F\rangle$  and the remaining atoms in the neighboring  $|F, m_F=\pm(F-1)\rangle$  state, where  $F=3$  or  $4$ . Feshbach resonances in four scattering states or channels can be thus studied:  $(3,3)+(3,3)$ ,  $(3,-3)+(3,-3)$ ,  $(4,4)+(4,4)$ , and  $(4,-4)+(4,-4)$ , where  $(F_1, m_{F1})+(F_2, m_{F2})$  indicates the collision of one atom in the  $|F_1, m_{F1}\rangle$  state with one in the  $|F_2, m_{F2}\rangle$  state.

We also prepare mixed samples containing atoms in two different internal states by either detuning the optical pumping beam or by applying an additional microwave pulse to transfer part of the population. Typically, we prepare 90% of the population in a stretched state  $|a\rangle$  and 10% in another state  $|b\rangle$ . After fully characterizing the collision properties of the  $(a)+(a)$  channel, the mixed collisions  $(a)+(b)$  can be monitored by either identifying resonances growing with the population in  $|b\rangle$  or by selectively detecting only the population in  $|b\rangle$ . The large population ratio of the two states ensures that  $(b)+(b)$  collision processes remain insignificant. Mixed scattering channels investigated in this work include  $(3,3)+(3,2)$ ,  $(3,3)+(4,4)$ ,  $(3,3)+(4,3)$ ,  $(3,3)+(4,2)$ ,  $(3,-3)+(3,-2)$ , and  $(4,-4)+(4,-3)$ .

The ability to study all these different scattering channels is crucial to provide information on the molecular bound states near the  $(F_1=3)+(F_2=3)$ ,  $(F_1=3)+(F_2=4)$ , and  $(F_1=4)+(F_2=4)$  hyperfine asymptotes. These span roughly 18 GHz in binding energy. As was shown in Ref. [15], the molecules have different characteristics near the three dissociation limits, which particularly helps determine the strength of the van der Waals interaction.

After the atoms have thermalized in the dipole trap, a uniform magnetic field up to 25 mT is applied. In order to preserve the atomic polarization during the field ramp, we first increase the field from  $14 \mu\text{T}$  to  $200 \mu\text{T}$  in 200 ms and then to an arbitrary field value in another 100 ms. The magnetic field experienced by the atoms is calibrated to an accuracy of  $\delta B < 0.1 \mu\text{T}$  at low field and  $\delta B/B < 10^{-4}$  at high field from the Zeeman splitting between magnetic sublevels, as measured with microwave spectroscopy [17]. Slowly changing stray fields of typically  $50 \mu\text{T}$  and remnant fields from the magnetized vacuum chamber up to  $2 \mu\text{T}$  are carefully canceled with six independent bias coils in three or-

thogonal directions to an accuracy of  $0.1 \mu\text{T}$  for the field and  $2 \mu\text{T}/\text{cm}$  for the field gradient. An effective magnetic field due to residual circular polarization of the YAG trapping beam [20] is monitored with microwave spectroscopy and reduced below  $0.05 \mu\text{T}$  by linearizing the beam polarization. To suppress the effects of field inhomogeneity and atomic density variation between the various YAG 1D lattice sites, we perform measurements only on the center portion of the cloud within  $\pm 0.4\sigma_z$ , which contains 900 lattice sites with a mean atomic density variation of  $< 10\%$ .

### III. INELASTIC FESHBACH SPECTROSCOPY

Inelastic collisions occur when the initial scattering state couples to open channels with lower internal energy; see Fig. 1. Due to energy conservation, the internal energy difference is converted into the relative kinetic energy of the atom pair and is either on the order of the ground-state hyperfine splitting or the Zeeman energy. In both cases, the energy release is generally much larger than our trap depth and therefore results in a loss of the colliding atom pair from the trap. Near a Feshbach resonance, inelastic loss is either enhanced or suppressed due to constructive or destructive interference between the off-resonant scattering amplitude with the on-resonant amplitude. In this work, we observe mostly enhanced inelastic collision processes and only one prominent suppression at 7.66 mT in the  $(3,3)+(4,2)$  incident scattering channel [17].

Experimentally, the inelastic rates are determined by fitting the mean atom density  $\bar{n}$  to  $d\bar{n}/dt = -L\bar{n} - K\bar{n}^2$ , where  $L$  is a one-body loss rate and  $K$  is the desired collision rate coefficient. If we assume that the atoms only reside in the harmonic region of the YAG dipole trap potential and that the cloud is in thermal equilibrium and at constant temperature  $T$  during the experiment, then the mean atom density is  $\bar{n} = N(m\bar{\omega}^2/4\pi k_B T)^{3/2}$  where  $N$  is the atom number in one lattice site,  $\bar{\omega} = \omega_z^{1/3} \omega_r^{2/3}$  is the mean vibration frequency,  $m$  is the cesium atomic mass, and  $k_B$  is the Boltzmann constant. The above differential equation can be solved analytically and directly relates the measured trap loss to the thermally averaged loss coefficient  $K$ . The one-body loss rate is the same for all measurements. A typical measurement is shown in Fig. 3 with a holding time up to 5 s.

The loss rates as a function of external magnetic field are measured by observing the atom loss within a holding time between 30 and 300 ms, such that the maximum collision loss is less than 30% and the atomic temperature varies by less than 10%. Slow variations in the initial atom number are monitored after every ten measurements and corrected for. On the other hand, to observe and locate weak resonances, we allow the atoms to interact for a longer time up to 500 ms in order to obtain better signal to noise. In this case, we ignore the temperature evolution and report only the fractional loss of atoms.

Collisions between atom pairs in two different internal states, such as  $(3,-3)+(3,-2)$ , differ from those in the same state in that both the even and odd partial waves can be scattered. In the  $(3,-3)+(3,-2)$  channel, for instance, we

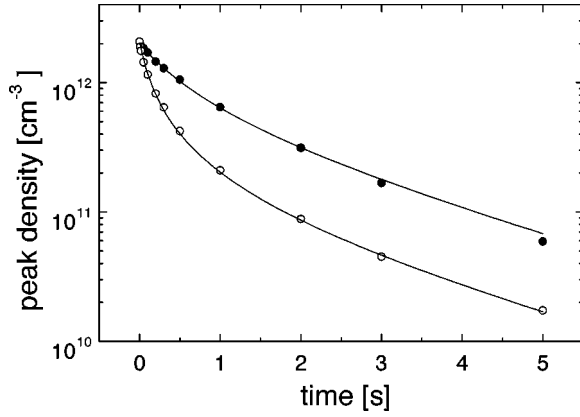


FIG. 3. Resonant and off-resonant time evolution of the atomic density. Atoms are prepared in  $|F=4, m_F=-4\rangle$  at  $T=5.3 \mu\text{K}$  and  $\bar{n} = 2.1 \times 10^{12} \text{ cm}^{-3}$  at  $B=14 \mu\text{T}$  (solid circles) and  $B=20.5 \text{ mT}$  (open circles), where a strong Feshbach resonance is located. See also Table I.

observe rich Feshbach spectra containing both  $s$ - and  $p$ -wave resonances.

The positions of the inelastic Feshbach resonances are tabulated in Tables I and II.

#### A. $(4,4)+(4,4)$ inelastic collisions

The stretched  $|4,4\rangle$  state was considered a promising candidate for reaching Bose-Einstein condensation in a magnetic trap before the cesium collision properties were revealed. Large inelastic losses that grow as the temperature is reduced were discovered that prevent the condensation of cesium in this state [25–27].

We find no resonance structure for a sample polarized in the  $|4,4\rangle$  state at  $5 \mu\text{K}$ , but a loss rate coefficient increasing slowly from  $2 \times 10^{-12} \text{ cm}^3 \text{ s}^{-1}$  to  $3 \times 10^{-12} \text{ cm}^3 \text{ s}^{-1}$  over the range of  $B=0\text{--}25 \text{ mT}$ . The absence of resonances in this channel is expected since the scattering channel  $(4,4)+(4,4)$  has the highest hyperfine and Zeeman energy of all ground-state hyperfine levels, and consequently Feshbach resonances cannot occur.

#### B. $(4,-4)+(4,-4)$ and $(4,-4)+(4,-3)$ inelastic collisions

We observe two narrow inelastic Feshbach resonances for collisions between two  $|4,-4\rangle$  atoms: a weak one at  $10.59 \text{ mT}$  and a strong one at  $20.50 \text{ mT}$ . In addition we have discovered an inelastic resonance in the  $(4,-4)+(4,-3)$  channel at  $20.66 \text{ mT}$ . The resonance field values have a ratio of 1:2:2 to within 3%. This ratio is not a coincidence, but a result of the molecular bound state structure below the continuum. See Table I. All three resonances are identified as originating from bound states with identical binding energy at zero magnetic field.

#### C. $(3,-3)+(3,-3)$ and $(3,-3)+(3,-2)$ inelastic collisions

The  $|3,-3\rangle$  state can be magnetically trapped and several attempts to reach BEC in this state were thwarted by the large collision loss [27]. In this work, we observe multiple

inelastic resonances for collisions between two such atoms, as shown in Fig. 4. One resonance at  $2.18 \text{ mT}$  is not identified; see Table II.

In  $(3,-3)+(3,-2)$  collisions, multiple  $s$ - and  $p$ -wave resonances are found and identified by varying the population in the  $|3,-2\rangle$  state, shown in Fig. 5. An alternative method to identify mixed-state resonances is based on detecting the population in  $|3,-2\rangle$  by microwave transitions on samples with 90% of the population in  $|3,-3\rangle$  and  $\sim 10\%$  in  $|3,-2\rangle$ . In this case, we observe an enhanced loss of the  $|3,-2\rangle$  population near inelastic collision resonances in the  $(3,-3)+(3,-2)$  channel and a suppressed loss of the  $|3,-2\rangle$  population near inelastic collision resonances in the  $(3,-3)+(3,-3)$  channel, the latter being due to the reduction in density of  $|3,-3\rangle$  atoms. This provides a clear distinction between the two collision processes.

#### D. $(3,3)+(3,3)$ and $(3,3)+(3,2)$ inelastic collisions

The  $(3,3)+(3,3)$  channel is the lowest hyperfine scattering channel and therefore has no binary exothermic collision processes. Collisional inelastic loss is then only due to three-body recombination, a process that falls outside the scope of this paper. A quantitative study of the recombination loss in the  $|3,3\rangle$  state is given in Ref. [28]. In collisions between  $|3,3\rangle$  and  $|3,2\rangle$  atoms we have observed no resonances below  $B=23.5 \text{ mT}$ . Theory predicts weak resonances that are beyond the sensitivity of our current experiment.

#### E. $(3,3)+(4,2)$ , $(3,3)+(4,3)$ , and $(3,3)+(4,4)$ inelastic collisions

Multiple Feshbach resonances due to  $(3,3)+(4,2)$  and  $(3,3)+(4,3)$  scattering are observed in samples with 80% population in  $|3,3\rangle$  and 15% in  $|4,3\rangle$  or  $|4,2\rangle$ . The remaining atoms are predominantly in the  $|3,2\rangle$  hyperfine state. We have verified that  $(3,3)+(3,2)$ ,  $(4,3)+(3,2)$ , and  $(4,2)+(3,2)$  processes do not contribute to the loss.

We prepare the sample by first polarizing 95% of the atoms in the  $|3,3\rangle$  state at  $B=14 \mu\text{T}$  and then applying a microwave pulse for a few ms, which selectively transfers approximately 15% of the population into  $|4,3\rangle$  or  $|4,2\rangle$ . Due to the almost identical energy splitting between the  $|3,3\rangle \leftrightarrow |4,2\rangle$  and  $|3,2\rangle \leftrightarrow |4,3\rangle$  microwave transitions at low field, we have a small population of  $|4,3\rangle$  in the experiment aimed at finding resonances in a  $(3,3)+(4,2)$  collision. Pollution by  $|3,3\rangle+|4,3\rangle$  resonances occurs, as was previously reported in Ref. [17].

We also observe a weak pollution by  $(3,3)+(4,2)$  resonances in the  $(3,3)+(4,3)$  spectrum. This cannot be explained by microwave transitions, since  $|3,3\rangle \leftrightarrow |4,3\rangle$  and  $|3,2\rangle \leftrightarrow |4,2\rangle$  do not have the same frequency. A possible process that creates atoms in the  $|4,2\rangle$  state is the inelastic collision process  $(3,2)+(4,3) \rightarrow (3,3)+(4,2)$ . At low fields the hyperfine and Zeeman energy difference between the final and initial states is  $\delta E = k_B 0.52 \mu\text{K} \times (B/\text{mT})$ . For our atomic temperatures and magnetic fields, this endothermal spin-changing collision can create atoms in the  $|4,2\rangle$  state.

TABLE I. Location and assignment of the observed Feshbach resonances. The first three columns define and give the results of the experiment, where the first column denotes the initial collision state, the second column indicates elastic (el.) or inelastic (inel.) measurements, and the third column is the experimental resonance location  $B_{\text{expt}}$ . The next four columns describe the quantum labels of the resonances. These are the partial wave of the initial collision state, the partial wave of the Feshbach state, the molecular spin  $f$ , and its projection  $m$  obtained from multichannel *bound-state* calculations. The last column gives the theoretical resonance location  $B_{\text{theor}}$  obtained from a multichannel *scattering* calculation at a collision energy of  $E/k_B=5.3 \mu\text{K}$ . The resonance at  $B_{\text{expt}}=20.66 \text{ mT}$  is extremely narrow and was not observed in the theoretical scattering calculation but nevertheless could be assigned from bound-state calculations. Several Feshbach resonances have ambiguous assignments (see text).

State	Experiment		Theory				$B_{\text{theor}}$ (mT)
	Method	$B_{\text{expt}}$ (mT)	Assignment	$l$	$f$	$m_f$	
			Inc. Wave				
(3,3)+(3,3)	el.	1.706(3) <sup>a</sup>	$s$	$s$	6	6	1.70(2)
(3,3)+(3,3)	el.	4.802(3) <sup>a</sup>	$s$	$d$	4	4	4.79(2)
(3,3)+(3,2)	el.	5.69(2) <sup>a</sup>	$s$	$d$	4	4	5.70(2)
(4,-4)+(4,-4)	inel.	10.590(3)	$s$	$d$	8	-6	10.58(2)
(4,-4)+(4,-4)	inel.	20.503(3)	$s$	$d$	8	-7	20.49(2)
(4,-4)+(4,-3)	inel.	20.66(1)	$s$	$d$	8	-6	
(3,-3)+(3,-3)	inel.	3.005(5)	$s$	$d$	6	$\approx -6$	2.99(2)
(3,-3)+(3,-3)	inel.	3.305(5)	$s$	$d$	6	-4	3.28(2)
(3,-3)+(3,-3)	inel.	8.69(2)	$s$	$d$	8	-8	8.80(2) <sup>b</sup>
(3,-3)+(3,-3)	inel.	10.11(2)	$s$	$d$	8	-7	10.15(2)
(3,-3)+(3,-3)	inel.	10.88(2)	$s$	$d$	8	-6	10.90(2)
(3,-3)+(3,-3)	inel.	11.81(2)	$s$	$d$	8	-5	11.85(2)
(3,-3)+(3,-3)	inel.	13.31(2)	$s$	$d$	8	-4	13.35(2)
(3,3)+(4,2)	inel.	6.17(2)	$s$	$d$	7	5	6.21(2)
(3,3)+(4,2)	inel.	7.66(2) <sup>c</sup>	$s$	$s$	6	5	7.53(2)
(3,3)+(4,2)	inel.	8.05(2)	$p$	$p$	6	5	8.08(2)
(3,3)+(4,2)	inel.	8.38(2)	$s$	$d$	7	6	8.43(2)
(3,3)+(4,2)	inel.	11.00(3)	$s$	$d$	7	5,7	11.02(2)
(3,3)+(4,2)	inel.	11.20(3)	$s$	$d$	7	5,7	11.20(2)
(3,3)+(4,2)	inel.	16.22(4)	$s$	$s$	5	5	16.23(2)
(3,3)+(4,2)	inel.	18.29(5)	$p$	$p$	5	5	18.45(2)
(3,3)+(4,3)	inel.	12.90(3)	$s$	$d$	7	6	12.96(2)
(3,3)+(4,3)	inel.	17.30(4)	$p$	$p$	6	6	17.45(2)
(3,3)+(4,3)	inel.	22.73(5)	$s$	$d$	7	5,7	22.75(2)
(3,3)+(4,3)	inel.	23.05(5)	$s$	$d$	7	5,7	23.13(2)

<sup>a</sup>Minimum evaporation rate.

<sup>b</sup>Temperature-dependent resonance occurred at  $\text{Re}(a)=0$ .

<sup>c</sup>Minimum inelastic loss.

The four resonances in the (3,3)+(4,2) channel at 6.17 mT, 8.38 mT, 11.0 mT, and 11.2 mT and all four resonances observed in the (3,3)+(4,3) channel at 12.9 mT, 17.3 mT, 22.7 mT, and 23.1 mT are paired with an identical ratio of the field values 2.07(2). This observation is confirmed by the theoretical identification of the paired resonances as being due to molecular states with identical binding energy at zero magnetic field.

In a separate experiment we have found no inelastic resonances in (3,3)+(4,4) collisions for magnetic field strengths up to 23.5 mT, in agreement with theory.

#### IV. ELASTIC FESHBACH SPECTROSCOPY

The resonant change of the scattering amplitude in the incident channel also results in a modification of the elastic cross section. We refer to this process as an elastic Feshbach resonance; see Fig. 1. Beside the direct measurement of the thermalization rate between the axial and radial motion [18,29], we have developed a more sensitive measurement technique for elastic Feshbach resonances: the measurement of the evaporation rate in a shallow trap [17]. This method converts the temperature evolution measurement into an

TABLE II. Feshbach resonances, continued. Columns defined as in Table I. One bound state could not be assigned while three resonances have not been observed experimentally.

State	Experiment		Theory				
	Method	$B_{\text{expt}}$ (mT)	Inc. Wave	$l$	$f$	$m_f$	$B_{\text{theor}}$ (mT)
(3,-3)+(3,-3)	inel.	2.18(2)					<sup>a</sup>
(3,-3)+(3,-2)	inel.	3.57(2)	$s$	$d$	6	-5	3.55(5)
(3,-3)+(3,-2)	inel.	10.50(1)	$p$	$f$	7	-7	10.50(5)
(3,-3)+(3,-2)	inel.	11.04(2)	$p$	$f$	7	-7	11.03(5)
(3,-3)+(3,-2)	inel.	11.39(2)	$p$	$f$	7	-7	11.35(5)
(3,-3)+(3,-2)	inel.	12.01(2)	$s$	$d$	8	-7	12.03(5)
(3,-3)+(3,-2)	inel.	13.01(2)	$s$	$d$	8	-6	13.05(5)
(3,-3)+(3,-2)	inel.	14.58(2)	$s$	$d$	8	-5	14.65(5)
(3,-3)+(3,-2)	inel.	17.02(2)	$s$	$d$	8	-4	17.05(5)
(3,-3)+(3,-2)	inel.		$s$	$d$	8	-3	20.88(5) <sup>b</sup>
(3,-2)+(3,-2)	inel.	14.82(2) <sup>c</sup>	$s$	$d$	8	-7	14.80(5)
(3,-2)+(3,-2)	inel.	16.58(2) <sup>c</sup>	$s$	$d$	8	-6	16.50(5)
(3,-2)+(3,-2)	inel.	19.25(2) <sup>c</sup>	$s$	$d$	8	-5	19.25(5)
(3,-2)+(3,-2)	inel.		$s$	$d$	8	-4	23.75(5) <sup>b</sup>
(3,-3)+(3,-1)	inel.	12.92(2)	$s$	$d$	8	-8	12.90(5)
(3,-3)+(3,-1)	inel.		$s$	$d$	8	-4	21.15(5) <sup>b</sup>

<sup>a</sup>Not predicted by calculation.

<sup>b</sup>Not observed experimentally.

<sup>c</sup>Has equal contribution from (3,-3)+(3,-1) collision.

atom number measurement, which provides better sensitivity and signal-to-noise ratio.

We report elastic collision properties in the pure (3,3)+(3,3) channel and in the mixed (3,3)+(3,2) channel, where the measurements are not complicated by inelastic processes. Although the elastic cross section can in principle be either enhanced or suppressed by the Feshbach resonance, we observe only dips in the the elastic collision rate at  $T$

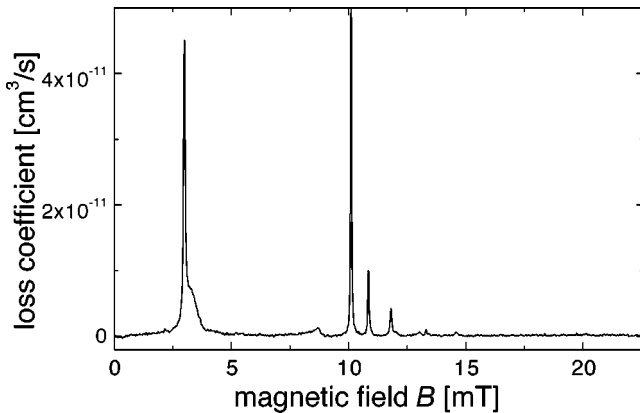


FIG. 4. Binary loss coefficient in a gas of  $|F=3, m_F=-3\rangle$  atoms as a function of external magnetic field. The initial mean atomic density is  $\bar{n}=5 \times 10^{12} \text{ cm}^{-3}$  at a temperature of  $\sim 5 \mu\text{K}$ . Populations in the  $|F=3, m_F=-3\rangle$ ,  $|F=3, m_F=-2\rangle$ , and all other states are 95%,  $\sim 5\%$ , and  $<1\%$ , respectively. Magnetic field resolution is  $10 \mu\text{T}$ .

$=5 \mu\text{K}$ . This is due to the large background scattering length, such that, at  $5 \mu\text{K}$ , the collision is not in the Wigner threshold regime [30]. The off-resonant cross section is already very close to the maximum value or the unitarity limit. In the (3,3)+(3,3) channel, a vanishing elastic collision

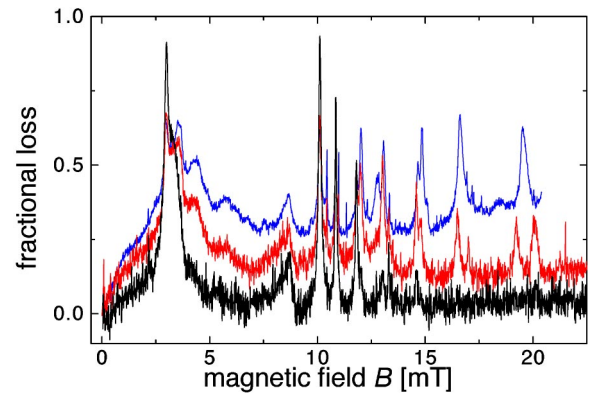


FIG. 5. Atom loss as a function of magnetic field for an initial mean density  $\bar{n}=5 \times 10^{12} \text{ cm}^{-3}$ , temperature of  $\sim 5 \mu\text{K}$ , and interaction time of 300 ms. Populations in the  $|F=3, m_F=-3\rangle$ ,  $|F=3, m_F=-2\rangle$ , and all other states are 95%,  $\sim 5\%$ , and  $<1\%$  for the lower curve, 85%,  $\sim 10\%$ , and  $\sim 5\%$  for the middle curve, and  $\sim 70\%$ ,  $\sim 20\%$ , and  $\sim 10\%$  for the upper curve, respectively. Comparison between the curves facilitates the identification of the incident channel responsible for the Feshbach resonances. Magnetic field resolution is  $10 \mu\text{T}$ .

cross section at 1.71 mT resulting from an *s*-wave Feshbach resonance was first observed as a strong reduction in the cross axis rethermalization rate [18]. One additional narrow *d*-wave Feshbach resonance at 4.80 mT is found by monitoring the evaporative loss rate of atoms in  $|3, 3\rangle$  state [17]. In the  $(3, 3)+(3, 2)$  channel, a minimum of the elastic collision rate at 5.7 mT is observed using the same evaporative loss method, when we measure the atom number in the  $|3, 2\rangle$  state. The positions of the elastic collision rate minima are given in Table I.

The elastic collision measurements based on evaporative loss are limited to resonances whose width in energy is comparable to or exceeds the thermal energy of the sample  $k_B T$ . For narrow resonances the resonant variation of the elastic collision rate over a small interval of collision energies does not lead to observable variations in the evaporation rate. For the detection of such weak resonances we have to resort to radiative Feshbach spectroscopy, discussed in the next section.

## V. RADIATIVE FESHBACH SPECTROSCOPY

Narrow resonances with a linewidth that is small compared to the thermal energy  $k_B T$  do not significantly affect the sample's thermalization rate and therefore cannot be probed by elastic Feshbach spectroscopy. However, it is possible to directly measure the enhanced (quasi)-bound-state population on a Feshbach resonance using a far-detuned laser beam to selectively dissociate the molecules, while leaving the atoms unperturbed. This technique is called radiative Feshbach spectroscopy [6,16].

In this work, we apply radiative Feshbach spectroscopy to probe Feshbach resonances in the  $(3, 3)+(3, 3)$  and  $(3, 3)+(3, 2)$  scattering channels using a probe beam typically detuned from 20 GHz to 4 THz to the blue of the cesium  $D_2$  transition at 852.3 nm. The probe beam is provided by a titanium-sapphire laser and uniformly illuminates the atom sample with a stabilized intensity up to 50 W/cm<sup>2</sup>. The intensity and detuning of the laser are adjusted such that the single-atom excitation is sufficiently weak to produce negligible atom loss when the magnetic field is tuned off the Feshbach resonances, while maximizing the loss on the Feshbach resonance.

To measure the radiative collision loss, we first prepare atom samples either fully polarized in the  $|3, 3\rangle$  to study  $(3, 3)+(3, 3)$  collisions or 85% in  $|3, 3\rangle$  and 15% in  $|3, 2\rangle$  to study  $(3, 3)+(3, 2)$  collisions. After the preparation and field ramping, we typically illuminate the atoms with the probe beam for  $t=100-300$  ms and measure the trap loss. To determine the radiative loss rate as a function of magnetic field, we perform two consecutive atom number measurements at every magnetic field value to discriminate nonradiative loss:  $N_1$  is the atom number at without the probe beam, and  $N_2$  is obtained at with the probe beam. The radiative loss rate is then given by  $\gamma=(1-N_2/N_1)/t$ , where the illumination time  $t$  is chosen to keep the maximum atomic loss below 30%. To increase the detection sensitivity to weak resonances, we lengthen  $t$  to  $>500$  ms and average each data point up to 5 times. A detailed spectrum thus obtained is shown in Fig. 6.

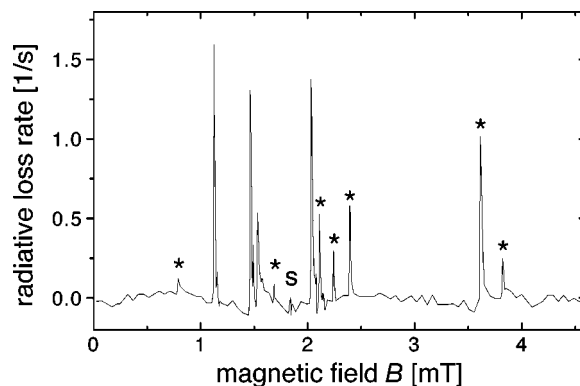


FIG. 6. A detailed radiative loss spectrum. The probe beam at wavelength  $\lambda=844$  nm has an intensity of 50 W/cm<sup>2</sup>. Here 85% (15%) of the atoms are in the  $|3, 3\rangle$  ( $|3, 2\rangle$ ) state. The temperature and mean density of the sample are 3.5  $\mu$ K and  $1 \times 10^{13}$  cm<sup>-3</sup>, respectively. “S” indicates a shape resonance; the stars indicate Feshbach resonances in the  $(3, 3)+(3, 2)$  channel. Magnetic field resolution near the resonances is 5  $\mu$ T.

The details of the radiative loss line shape are discussed in Ref. [16]; atom-molecule dynamics and the sensitivity of the our radiative Feshbach spectroscopy are studied in Ref. [6]. The positions of the resonances are tabulated in Table III. Two of the Feshbach resonances observed by radiative Feshbach spectroscopy was recently used to create ultracold cesium molecules [6,7].

## VI. THEORY

The structure of the Hamiltonian of two interacting <sup>2</sup>S ground-state alkali-metal atoms is well known. It contains the atomic kinetic energy operator, an atomic Hamiltonian for each atom, two Born-Oppenheimer potentials with symmetry <sup>1</sup> $\Sigma_g^+$  and <sup>3</sup> $\Sigma_u^+$ , the nuclear rotation operator  $\hbar^2 \vec{l}^2 / (2\mu R^2)$ , and weaker relativistic spin-spin dipole and second-order spin-orbit interactions. Here  $\vec{l}$  is the nuclear mechanical angular momentum and  $\mu$  is the reduced mass of the molecule.

The atomic Hamiltonian contains a Fermi contact term and the Zeeman interaction when an external magnetic field  $B$  directed along the  $z$  axis is present during the collision. The eigenstates of the  $B=0$  atomic Hamiltonian are  $|F_\alpha, m_{F_\alpha}\rangle$ , where  $\alpha=1$  or 2 for atom 1 or 2,  $\vec{F}_\alpha = \vec{s}_\alpha + \vec{i}_\alpha$ , and  $m_{F_\alpha}$  is the projection of  $\vec{F}_\alpha$  along the  $z$  axis. Here  $\vec{s}_\alpha$  and  $\vec{i}_\alpha$  are the atomic electron and nuclear spins, respectively. For  $B>0$ , states with the same  $m_{F_\alpha}$  mix,  $F_\alpha$  is no longer a good quantum number, and the zero-field  $m_{F_\alpha}$  degeneracy is lifted. For convenience, atomic eigenstates in a magnetic field will be labeled by  $|F_\alpha, m_{F_\alpha}\rangle$  since for the fields used in this paper the Zeeman interaction is small compared to the hyperfine interaction and  $F_\alpha$  is an approximately good quantum number. We use hyperfine constants and magnetic moments from Ref. [31]. The nuclear spin of cesium is 7/2.

The selection rules for the Born-Oppenheimer Hamiltonian conserve  $\vec{l}$  and  $\vec{f} = \vec{F}_1 + \vec{F}_2$ . Consequently, bound states and scattering amplitudes can be labeled by  $fl$  for  $B=0$  and

TABLE III. Feshbach resonances and a single shape resonance observed with radiative spectroscopy. Columns defined as in Table I. Several Feshbach resonances have ambiguous assignments (see text).

State	Experiment		Theory				
	Method	$B_{\text{expt}}$ (mT)	Assignment				
			Inc. Wave	$l$	$f$	$m_f$	$B_{\text{theor}}$ (mT)
(3,3)+(3,3)	rad.	1.102(3)	$s$	$g$	4	2	1.12(2)
(3,3)+(3,3)	rad.	1.437(3)	$s$	$g$	4	3	1.46(2)
(3,3)+(3,3)	rad.	1.506(3)	$s$	$g$	6	5	1.51(2)
(3,3)+(3,3)	rad.	1.83(1)	$s$	$d$			1.86(2) <sup>a</sup>
(3,3)+(3,3)	rad.	1.990(3)	$s$	$g$	4	4	2.01(2)
(3,3)+(3,3)	rad.	4.797(3)	$s$	$d$	4	4	4.77(2)
(3,3)+(3,3)	rad.	5.350(3)	$s$	$g$	2	2	5.43(2)
(3,3)+(3,3)	rad.	11.278(3)	$s$	$d$	6	4	11.32(2)
(3,3)+(3,3)	rad.	13.106(3)	$s$	$d$	4	4	13.19(2)
(3,3)+(3,2)	rad.	0.78(1)	$s$	$g$	6	3	0.83(2)
(3,3)+(3,2)	rad.	1.13(1)	$s$	$g$	4	1	1.17(2)
(3,3)+(3,2)	rad.	1.47(1)	$s$	$g$	4 2 or 6 4		1.54(2)
(3,3)+(3,2)	rad.	1.66(1)	$p$	$f$	3	2	1.64(2)
(3,3)+(3,2)	rad.	2.09(1)	$s$	$g$	4	3	2.16(2)
(3,3)+(3,2)	rad.	2.21(1)	$p$	$f$	1 1 or 3 3		2.18(2)
(3,3)+(3,2)	rad.	2.36(1)	$p$	$f$	1 1 or 3 3		2.33(2)
(3,3)+(3,2)	rad.	3.60(1)	$s$	$g$	4	4	3.70(2)
(3,3)+(3,2)	rad.	3.81(1)	$p$	$f$	5	1	3.78(2)
(3,3)+(3,2)	rad.	4.68(1)	$p$		$f$ 5 2 or $p$ 5 4,5		4.70(2)
(3,3)+(3,2)	rad.	4.93(1)	$p$		$f$ 5 2 or $p$ 5 4,5		4.89(2)
(3,3)+(3,2)	rad.	4.99(1)	$p$		$f$ 5 2 or $p$ 5 4,5		4.99(2)
(3,3)+(3,2)	rad.	5.70(1)	$s$	$d$	4	4	5.70(2)
(3,3)+(3,2)	rad.	5.77(1)	$p$	$p$	5	3,4,5	5.78(2)
(3,3)+(3,2)	rad.	5.87(1)	$p$	$p$	5	3,4,5	5.86(2)
(3,3)+(3,2)	rad.	5.97(1)	$p$	$p$	5	3,4,5	5.98(2)

<sup>a</sup> $d$ -wave shape resonance.

$m_f l$  for  $B > 0$ . Here,  $m_f = m_{F1} + m_{F2}$ . The two relativistic interactions weakly mix states with different  $l$  and  $f$ . Global symmetries ensure that the molecular Hamiltonian, including the relativistic interactions, conserves parity and total angular momentum  $\vec{F} = \vec{f} + \vec{l}$  and its projection  $M = m_f + m_l$  for  $B = 0$  or only  $M$  for nonzero fields. Only even or odd partial waves are coupled. For  $B = 0$  there are at most 72 coupled channels while for nonzero fields there are infinitely many coupled channels. In practice the number of channels is restricted by using knowledge about the relative strengths of the individual terms in the Hamiltonian.

The relativistic interactions, even though weak, are crucial in understanding the presence of  $d$ -wave and  $g$ -wave Feshbach resonances in our gas of ultracold Cs atoms. The temperature  $T \approx 5 \mu\text{K}$  is small compared to the 200  $\mu\text{K}$  and 1 mK barrier height of the  $d$  and  $g$  partial waves, respectively, and only incoming  $s$ -wave and  $p$ -wave collisions contribute to the experimental signal. Coupling from the incoming  $s$ -wave to  $d$ - and  $g$ -wave bound states is induced by the relativistic interactions and is denoted as  $d$ - and  $g$ -wave Fes-

hbach resonance. Notice that  $g$ -wave Feshbach resonances are induced by higher-order spin-orbit interactions and therefore have very narrow resonance widths of a few  $10^{-7}$  T. The outgoing state is either  $s$ -wave in the scattering channel for elastic processes or some low partial waves in other channels for inelastic processes.

## VII. NUMERICAL APPROACHES

The scattering properties and bound-state energies of the ground-state Hamiltonian are obtained with two separate numerical approaches. Scattering wave functions and the scattering matrix at energy  $E$  are found using a Gordon propagator [32]. From the scattering matrix elastic and inelastic rate coefficients can be obtained. The relation between the scattering matrix and the rate coefficients is given in Ref. [33]. Feshbach resonances appear as sharp peaks or dips in the magnetic field dependence of the rate coefficients. For comparison with the experiments the rate coefficients need to be thermally averaged.

Obtaining discrete bound states with the Gordon method is cumbersome since eigenenergies are not *a priori* known and multichannel scattering wave functions need to be calculated at a large number of energies  $E$ . Consequently, a discrete variable representation [34] for the radial kinetic energy operator is used to find the bound states. In this approach the eigenvalues of a linear system of size given by the number of radial collocation points times the number of coupled channels need to be calculated. This can be done with standard linear algebra packages. However, resource limitations tend to restrict the number of coupled channels that can be conveniently handled. For the heavy cesium dimer a realistic maximum number of channels lies between 10 and 15, although 20 channels can still be treated. An interesting alternative for finding bound-state energies, which does not require the storage of the linear system, can be based on the multichannel quantum defect theory [35]. It takes advantage of analytic properties of wave functions as a function of energy  $E$  in order to limit the number of wave function evaluations.

Bound states are calculated over a range of magnetic field values. Feshbach resonances occur when a bound state crosses a collisional threshold. Examples of resonances can be found in Refs. [36,37]. In the absence of the two relativistic interactions calculations label individual bound states by  $m_f$ ,  $l$ , and  $M$ . In addition, the field dependence of a level can be traced to a bound state at zero field. At zero field  $f$  labels the bound states. For the magnetic fields used in our experiment  $f$  remains approximately good. Coupling of states with different  $m_f$  but the same  $l$  is sometimes needed to fully assign the Feshbach resonances. For this paper bound-state calculations are used to assign quantum numbers to the resonances.

The Feshbach resonances are experimentally observed in either elastic cross sections, inelastic rate coefficients, or radiative collision rates. The former two measurements can be modeled from first-principles scattering calculations of cross sections and rate coefficients. In principle the rate coefficients need to be thermally averaged. However, a proper thermalization was impractical and for a comparison between theory and experiment only a single collision energy given by the mean collision energy of a gas at temperature  $T$  was used. A combination of narrow Feshbach resonances and the need to study the effect of variations in the shape of the two Born-Oppenheimer potentials on the resonance locations would lead to an untenable number of scattering calculations. A one-standard-deviation uncertainty of 0.02–0.05 mT in the calculated magnetic field location of the Feshbach resonances observed in elastic or inelastic rates results from the use of a single collision energy.

The radiative collision data require modeling of the rate coefficient for the absorptions of a photon by a pair of ultracold Cs atoms [38]. However, we are interested in reproducing the location of Feshbach resonances, and not in the absolute absorption rates. Consequently, from a theoretical perspective it is sufficient to locate the resonances in the elastic cross section in the absence of light. The  $l=4$  ( $g$ -wave) resonances observed by radiative Feshbach spectroscopy could not be observed by direct measurement of the elastic cross section.

The energy widths of  $l=4$  ( $g$ -wave) Feshbach resonances are significantly smaller than the average collision energy. As a consequence, the location of the maximum of the photoassociation line shape as a function of magnetic field depends on the zero-collision-energy resonance field location  $B_0$ , the temperature, and the magnetic moment  $\mu_{\text{res}}$  of the embedded bound state. In practice, however, we located the resonances from scattering calculations at  $E/k_B=5.3 \mu\text{K}$  and used the magnetic moment of the  $g$ -wave Feshbach resonance obtained from bound-state calculations to extrapolate to zero collision energy.

## VIII. RESULTS

Tables I–III give the magnetic field locations and assignments of the observed Feshbach resonances. The numbers in parentheses indicate the one-standard-deviation uncertainty. The locations of the resonances are obtained from elastic and inelastic cross-section measurements or radiative spectroscopy. The theoretical resonance locations are obtained from coupled-channel scattering calculations at a  $E/k_B=5.3 \mu\text{K}$  collision energy and Born-Oppenheimer potentials with dispersion coefficients  $C_6=6890E_H a_0^6$  and  $C_8=954600E_H a_0^8$  and scattering lengths  $a_S=280.3a_0$  and  $a_T=2405a_0$  [15]. Here  $k_B$  is the Boltzmann constant,  $1E_H=4.35974 \text{ aJ}$  is one hartree, and  $1a_0=0.0529177 \text{ nm}$  is one Bohr radius. Here  $k_B 5.3 \mu\text{K}$  is the average collision energy for a Cs gas at  $T=3.5 \mu\text{K}$ . For resonances observed in the elastic (inelastic) rates the minimum (maximum) of the line is quoted. The only exception is the resonance at 7.66 mT, where the position of the minimum inelastic rate is given. For the resonances observed by radiative spectroscopy the maximum of the loss rate and the maximum of the theoretical inelastic collision rate in the absence of laser light are presented.

It should be noted that the magnetic field values for the spectral features presented here should not be confused with the location of the molecular Feshbach state introduced in Fig. 1. Typically, the molecular state can be defined anywhere within the width of the resonance.

The theoretical uncertainties are a consequence of our limited ability to model the experiments and are obtained by combining the uncertainties due to the spread in collision energies of a thermal Cs gas with the magnetic field dependence of the Feshbach resonance. Any discrepancy between theory and experiment in the tables that lies outside the error bars indicates deficiencies in the shape of the two Born-Oppenheimer potentials.

The assignment of the resonances is obtained by combining information from scattering and bound-state calculations. The initial collision partners that lead to a resonance are determined from theoretical scattering calculations and experimentally by varying the relative population of hyperfine states in the Cs gas and comparing the relative strength of the resonances. The incoming partial wave is obtained from scattering calculations. The assignment of quantum numbers  $l$ ,  $f$ , and  $m_f$  is made on the basis of bound-state calculations. One resonance could not be assigned.

Levels with the same  $l, f, m_f$  symmetry but different  $M = m_l + m_f$  are degenerate except for small splittings from the

second-order spin-orbit and spin-spin interactions. For even partial waves this is not an issue as losses from the  $s$ -wave entrance channel at collision energies of the order of a few microkelvin are much larger than those from  $d$ -wave entrance channels and thus only resonances with  $M$  equal to the sum of the magnetic quantum number of the initial hyperfine states,  $M=m_{f1}+m_{f2}$ , are observed. For collisions between atoms in unlike hyperfine states contributions from  $p$ -wave collisions cannot be ignored and nearly degenerate Feshbach resonances from three  $M$  values appear.

A good example of the complexity for odd- $l$  resonances can be found between 4.0 mT and 6.0 mT in the radiative Feshbach spectrum from a  $(3,3)+(3,2)$  collision. In this region six nearly degenerate resonances are labeled  $l=f$ ,  $f=5$ ,  $m_f=2$ , or  $l=p$ ,  $f=5$ . The  $m_f$  labels of the  $p$ -wave resonance could not be assigned. It turns out that this resonance has a small magnetic moment and at  $B \approx 5$  mT the different  $m_f$  components are nearly degenerate. Mixing between different  $m_f$  components for the same  $M$  due to second-order spin-orbit and spin-spin interactions leads to shifts that are comparable to the spacings due to the Zeeman interaction. The  $l=f$  resonances, which have a larger magnetic moment, accidentally reside in the same magnetic field region.

We have assigned more than one set of labels to the resonances between 4.0 mT and 6.0 mT, because  $m_f$  and to a lesser degree  $l$  and  $f$  are not good quantum labels. There are eight different  $l=p$ ,  $f=5$  and  $l=f$ ,  $f=5$ ,  $m_f=2$  resonances between 4.0 mT and 6.0 mT. Six of these eight resonances are due to the  $p$ -wave symmetry. This can easily be checked by noting that only  $M=4$ , 5, and 6 can lead to these odd- $l$  resonances. Not all eight resonances have been seen, which might be due to the fact that some are not resolved or unobserved by radiative spectroscopy. We did not perform quantitative *bound-state* calculations as too many channels must be coupled together. The theoretical field locations listed in the last column of the tables have been obtained from scattering calculations where all states are included at the cost of losing the ability to assign quantum labels.

Figure 7 shows even- $l$   $M=6$  bound states below the lowest molecular hyperfine state  $(3,3)+(3,3)$  as a function of magnetic field. Each bound state is labeled with  $f$  and  $l$ . A resonance occurs when a bound state crosses zero energy. The frequency range shown in the figure is sufficient for the assignment of all  $B < 15$  mT  $s$ -,  $d$ -, and  $g$ -wave Feshbach resonances in the collision between  $|3,3\rangle$  Cs atoms. The solid circles mark the observed threshold resonances in a Cs gas at  $T=3.5$   $\mu$ K ( $k_B T/h \approx 0.1$  MHz). Agreement between theory and experiment is sufficiently good that assignments can be made even though discrepancies exist. These discrepancies are caused by the (slightly) incorrect shape of the Born-Oppenheimer potentials and the approximations in the bound-state calculations. For fields smaller than 1 mT theory predicts the existence of additional resonances.

The number of coupled channels for  $M=6$  and  $l=s, d$ , and  $g$  is 74. However, as discussed in the previous section, for nonzero applied magnetic field the coupling between different partial waves and  $m_f$ 's is due to weak second-order spin-orbit and spin-spin interactions. Consequently, for most resonances in Fig. 7 the assignment is unambiguous using independent bound-state calculations that only include states

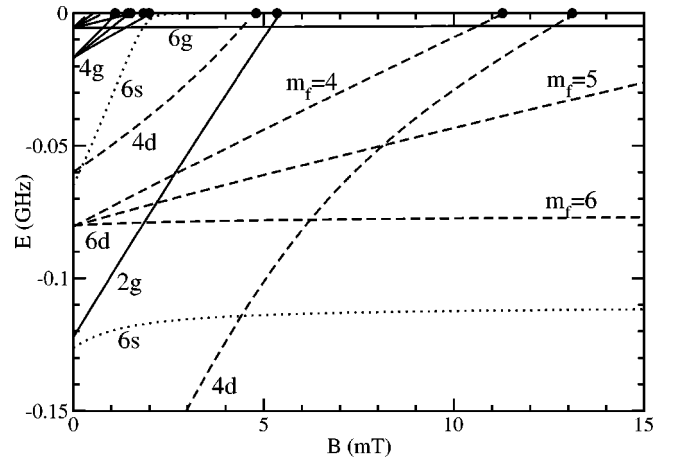


FIG. 7. Total angular momentum projection  $M=6$ ,  $s$ -,  $d$ -, and  $g$ -wave bound state energies as a function of magnetic field. The zero of energy corresponds to the  $(F=3, m_F=3) + (F=3, m_F=3)$  dissociation limit. Dotted, dashed, and solid lines correspond to  $l=s, d$ , and  $g$  states, respectively. Furthermore, each curve is labeled by the quantum numbers  $fl$ —i.e.,  $fl=6s$ . The molecular spin  $f$  is a zero-field quantum number. For the  $fl=6d$  states the magnetic quantum number  $m_f$  is also indicated. The solid circles represent the observed threshold resonances.

of a given  $l$  and  $m_f$ . In fact, the curves in the figure have been obtained in this way. However, it should be realized that the crossings between bound states shown in the figure are actually avoided when second-order spin-orbit and spin-spin interactions are included. At zero magnetic field coupling between channels with different molecular spin  $f$  is also small. The assignment of  $f$  is obtained by retracing a bound state to a zero magnetic field and noting that  $|m_f| \leq f$ .

A close look at Fig. 7 shows that the lines can roughly be divided into those that are noticeably curved and those that appear straight. A good example of curved lines is the two  $fl=4d$  bound states, while the  $6d$  and  $4g$  bound states are good examples of bound states that have a linear magnetic field dependence. The curved lines are due to broad avoided crossings that appear because the same  $fl$ -labeled states readily mix when a magnetic field is applied. Mixing is due to the interplay of hyperfine, Born-Oppenheimer, and Zeeman interactions and is significantly larger than in avoided crossings mediated by second-order spin-orbit and spin-spin interactions.

The most weakly bound  $fl=6s$  state is bound by about 65 MHz at zero magnetic field, rises rapidly until it turns over near 2 mT, and then continues just below the dissociation limit. This avoided crossing is also shown in Fig. 8. The bound state does not run parallel to the dissociation limit. It becomes a Feshbach resonance near  $B=50$  mT. The behavior of this bound state has direct consequences for the  $s$ -wave scattering length of two  $|f_a m_a\rangle = |3,3\rangle$  atoms. Below 1.7 mT the scattering length is negative and above this field value it is positive. This zero of the scattering length has been observed in Ref. [18] and has been used to optimize the Born-Oppenheimer potentials in Refs. [15,17], as well as in this paper. It is interesting to realize that, as discussed in Ref. [15], for  $B < 1.7$  mT,  $d$ -wave channels affect the elastic scat-

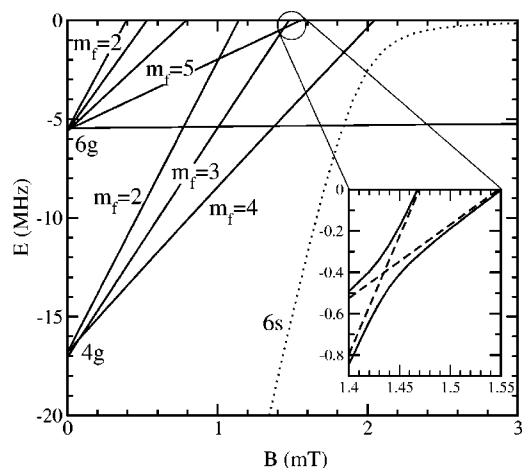


FIG. 8. Expanded view of the  $M=6$ ,  $s$ -,  $d$ -, and  $g$ -wave bound states shown in Fig. 7. An avoided crossing between  $g$ -wave  $m_f=3$  and  $5$  bound states occurs around  $B=1.4$  mT.

tering and must be included in order to obtain an accurate scattering length.

Some of the  $M=6$  and  $l=s, d$ , and  $g$  Feshbach resonances below  $B=3$  mT could at first not be assigned from calculations using states with the same  $l$  and  $m_f$ . Resonances of different  $lm_f$  symmetry lie in the same magnetic field region. Figure 8 shows a blowup of the 0–3 mT magnetic field range. The  $f=4$ ,  $m_f=3$ , and  $f=6$ ,  $m_f=5$   $g$ -wave bound states cross just below the dissociation limit and weak couplings might shift the corresponding Feshbach resonances. The inset shows the avoided crossing between these  $f=4$ ,  $m_f=3$ , and  $f=6$ ,  $m_f=5$   $g$ -wave bound state when the weak coupling between the two bound states is included. From the figure it is clear that the avoided crossing has little influence on the location of the Feshbach resonances and an  $fm_f$  label for each resonance can still be assigned.

The Born-Oppenheimer potentials that have been used for the theoretical resonance locations quoted in Tables I–III and Figs. 7 and 8 are based on the fit in our previous work [15], where the major uncertainties in the calculation of resonance positions arise from the poorly constrained  $C_8$  coefficient. For this paper we have improved the Born-Oppenheimer potentials by optimizing the  $C_8$  dispersion coefficient in addition to the  $C_6$  coefficient, the strength of the second-order spin-orbit interaction  $S_C$ , and the singlet and triplet scattering lengths [15]. For a given  $C_8$  the potentials are optimized to fit the minima in the elastic scattering rate of the  $(3,3)+(3,3)$  scattering at 1.706 mT and 4.802 mT, the  $f=6$   $d$ -wave resonance in  $(3,-3)+(3,-3)$  scattering at 3.005 mT, and the resonance in  $(4,-4)+(4,-4)$  scattering at 20.503 mT. Over a 10% range of the  $C_8$  coefficient near  $900\,000 E_H a_0^8$  a linear relationship between  $C_6$ ,  $S_C$ ,  $a_S$ , and  $a_T$  exists.

An improved cesium-dimer Hamiltonian is created by fitting to selected  $(3,3)+(3,3)$   $g$ -wave resonances. Figure 9 shows the  $M=6$ ,  $f=6$ ,  $m_f=5$ , and  $f=4$ ,  $m_f=3$ ,  $g$ -wave resonance position as a function of  $C_8$  or, equivalently,  $C_6$ . The figure shows theoretical zero-collision-energy resonance locations derived from  $E/k_B=5.3$   $\mu\text{K}$  calculations and the

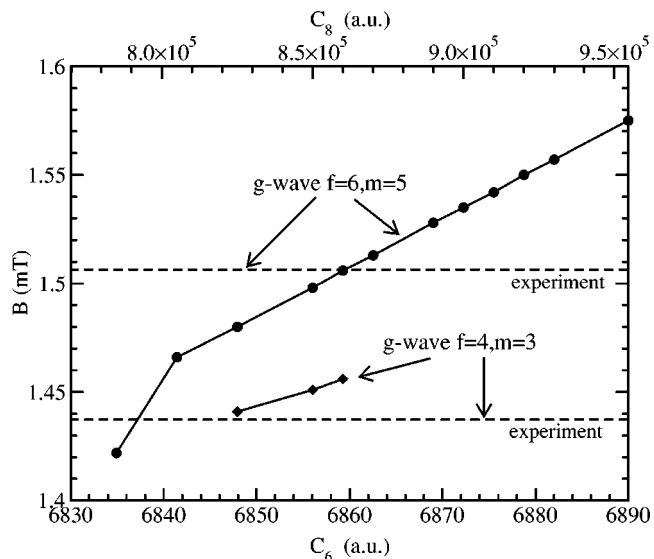


FIG. 9. Position of two  $M=6$   $g$ -wave resonances as a function of  $C_8$  or equivalently  $C_6$  for a zero-energy collision of two Cs atoms in the lowest hyperfine state. The  $C_6$  and  $C_8$  are expressed in units of  $E_H a_0^6$  and  $E_H a_0^8$ , respectively. The dotted lines correspond to the peak of the experimental radiative Feshbach spectroscopy signal.

magnetic moments of the resonances. The peak radiative detection signal as a function of magnetic field is due to collisions at zero energy. The magnetic moment of the resonances is  $170$   $\mu\text{K}/\text{mT}$  for the  $f=6$ ,  $m_f=5$  and  $550$   $\mu\text{K}/\text{mT}$  for the  $f=4$ ,  $m_f=3$  state.

The location of the Feshbach resonance found from a bound-state calculation, including only  $g$ -wave  $m_f=3$  and  $5$  channels, and a scattering calculation at zero collision energy, which includes *all*  $s$ -,  $d$ -, and  $g$ -wave channels, disagree by about  $0.02$  mT. This discrepancy is likely due to the limited number of channels in the bound-state calculations. The magnetic moments, however, are not expected to be significantly modified.

Table IV summarizes our best fit. Based on the collision parameters, cold collision properties of cesium atoms can be readily calculated in various scattering channels. In particular, the  $(3,3)+(3,3)$  and  $(3,-3)+(3,-3)$  scattering lengths

TABLE IV. Properties of the singlet  $X^1\Sigma_g^+$  and triplet  $a^3\Sigma_u^+$  Born-Oppenheimer potentials and the second-order spin-orbit interaction that give the best fit to all data on collisions between ultracold Cs atoms. The  $C_6$  and  $C_8$  are expressed in units of  $E_H a_0^6$  and  $E_H a_0^8$ , respectively. The singlet,  $a_S$ , and triplet,  $a_T$ , scattering lengths are in units of  $a_0$ . Here  $S_C$  is dimensionless. One-standard-deviation uncertainties are given.

	Value	Uncertainty (%)
$C_6$	6860	0.36
$C_8$	860 000	8.7
$a_S$	280.37	0.02
$a_T$	2440	1.0
$S_C$	2.6	19

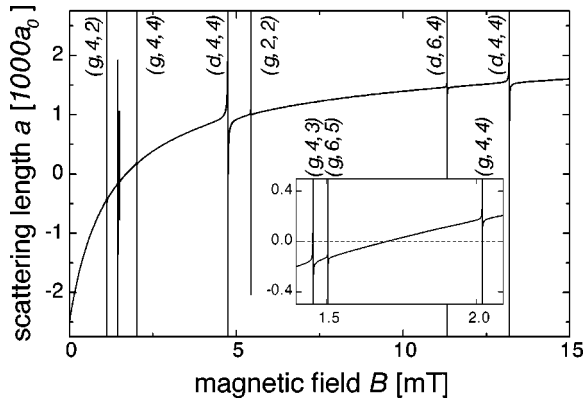


FIG. 10. Scattering length in the  $(F=3, m_F=3)+(F=3, m_F=3)$  scattering channel. Resonances resulting from the  $M=6$ ,  $s$ -,  $d$ -, and  $g$ -wave bound states are assigned with quantum number  $(l, f, m_f)$ , where  $l$  is the orbital angular momentum,  $f$  is the total internal angular momentum, and  $m_f$  is the magnetic quantum number. Calculations are done with a magnetic field grid size of  $50 \mu\text{T}$  for off-resonance regions and  $100 \text{ nT}$  near the narrow resonances. The inset shows the resonance structure near  $17 \text{ G}$  in detail.

are  $-2510 a_0$  at zero magnetic field. In the presence of the magnetic field, Fig. 10 shows the scattering length of the  $(3, 3)+(3, 3)$  channel as a function of magnetic field; Fig. 11 shows the collision rate constants in the  $(3, -3)+(3, -3)$  channel at the collision energy of  $E=k_B 1 \text{ nK}$ . All  $s$ -,  $d$ -, and  $g$ -wave channels are included in the calculation. These two states are particularly interesting in the experiments of cesium Bose-Einstein condensation [39]. The resonances are identified and labeled by the quantum numbers of the associated molecular states.

## IX. CONCLUSION

We have measured  $>60$  magnetic-field-induced Feshbach resonances in the collision of ultracold ground-state cesium atoms. Of all the alkali-metal species cesium is shown to have the richest resonance structure.

The field resonances have been observed in elastic collision rates, evaporation loss rates, collision relaxation rates, as well as in radiative collision resonance experiments (radiative Feshbach spectroscopy). The last experiments have been instrumental in observing  $l=4$   $g$ -wave Feshbach resonances with several  $0.1 \mu\text{T}$  resonance width.

Based on the previous work [15], we have improved the model for Cs-Cs collisions and in addition used multichannel bound-state calculations to assign each Feshbach resonance with pertinent quantum numbers. The quantum numbers correlate each resonance to a molecular bound state at zero magnetic field. We identify 3  $s$ -wave, 6  $p$ -wave, 32  $d$ -wave,

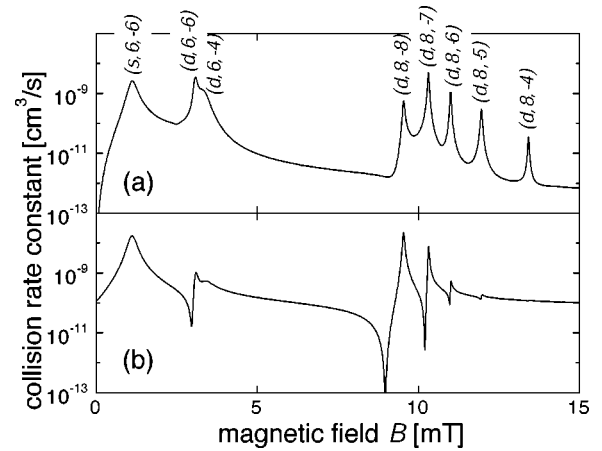


FIG. 11. Collision rate constants in the  $(F=3, m_F=-3)+(F=3, m_F=-3)$  scattering channel at  $E/k_B=1 \text{ nK}$ . Inelastic collision rates (a) and elastic collision rates (b) are calculated with a magnetic field grid size of  $10 \mu\text{T}$  for off-resonance regions and  $1 \mu\text{T}$  near the resonances. Resonances from the  $M=-6$ ,  $s$ -,  $d$ -, and  $g$ -wave bound states are included and assigned with quantum number  $(l, f, m_f)$ , where the notation is the same as in Fig. 10.

10  $f$ -wave, and 10  $g$ -wave Feshbach resonances and one shape resonance. One resonance in the  $(3, -3)+(3, -3)$  channel could not be identified and is possibly a three-body collision resonance or a two-body Feshbach resonance with very high partial-wave number.

The model has been used to calculate the molecular energy structure below the  $(F=3)+(F=3)$  continuum and the collision properties in the  $(3, 3)+(3, 3)$  and  $(3, -3)+(3, -3)$  scattering channels. These data will provide crucial information for experiments on cesium Bose-Einstein condensation [39] and cesium molecules [7].

In general, this paper presents the results of a successful collaboration of experimental and theoretical works and resolves the collision anomalies of cesium atoms. The excellent agreement on  $>60$  resonances between experiment and theory with only 5 parameters marks a triumph of the predictive power of atomic interaction theory. The experimental determination of the resonance locations is better than the theoretical estimate. Further improvements would require more flexibility in the (short-range shape) of the two Born-Oppenheimer potentials. Moreover, theoretical modeling will need to use thermally averaged elastic and inelastic rates as well as an improved model of the radiative line shape.

## ACKNOWLEDGMENTS

C.C. would like to thank P.S. Julienne for discussions. This work was supported in part by grants from the AFOSR and NSF.

- [1] E. Tiesinga, B. J. Verhaar, and H. T. C. Stoof, *Phys. Rev. A* **47**, 4114 (1993).
- [2] S. Inouye, M. Andrews, J. Stenger, H.-J. Miesner, S. Stamper-Kurn, and W. Ketterle, *Nature (London)* **392**, 151 (1998).
- [3] E. A. Doney, N. R. Claussen, S. L. Cornish, J. L. Roberts, E. A. Cornell, and C. E. Wieman, *Nature (London)* **412**, 295 (2001).
- [4] E. A. Donley, N. R. Claussen, S. T. Thompson, and C. E. Wieman, *Nature (London)* **417**, 529 (2002).
- [5] L. Khaykovich, F. Schreck, G. Ferrari, T. Bourdel, J. Cubizolles, L. D. Carr, Y. Castin, and C. Salomon, *Science* **296**, 1290 (2002); K. E. Strecker, G. B. Partridge, A. G. Truscott, and R. G. Hulet, *Nature (London)* **417**, 150 (2002).
- [6] C. Chin, A. J. Kerman, V. Vuletić, and S. Chu, *Phys. Rev. Lett.* **90**, 033201 (2003).
- [7] J. Herbig, T. Kraemer, M. Mark, T. Weber, C. Chin, H.-C. Nägerl, and R. Grimm, *Science* **301**, 1510 (2003).
- [8] C. A. Regal, C. Ticknor, J. L. Bohn, and D. S. Jin, *Nature (London)* **424**, 47 (2003); K. E. Strecker, G. B. Partridge, and R. G. Hulet, *Phys. Rev. Lett.* **91**, 080406 (2003); J. Cubizolles, T. Bourdel, S. J. J. M. F. Kokkelmans, G. V. Shlyapnikov, and C. Salomon, *ibid.* **91**, 240401 (2003); S. Jochim, M. Bartenstein, A. Altmeyer, G. Hendl, C. Chin, J. Hecker Denschlag, and R. Grimm, *ibid.* **91**, 240402 (2003); K. Xu, T. Mukaiyama, J. R. Abo-Shaer, J. K. Chin, D. E. Miller, and W. Ketterle, *ibid.* **91**, 210402 (2003).
- [9] S. Jochim, M. Bartenstein, A. Altmeyer, G. Hendl, S. Riedl, C. Chin, J. Hecker Denschlag, and R. Grimm (unpublished); M. Greiner, C. A. Regal, and D. S. Jin, *Nature (London)* **426**, 537 (2003); M. W. Zwierlein, C. A. Stan, C. H. Schunck, S. M. F. Raupach, S. Gupta, Z. Hadzibabic, and W. Ketterle, *ibid.* **91**, 250401 (2003).
- [10] K. Gibble and S. Chu, *Phys. Rev. Lett.* **70**, 1771 (1993).
- [11] M. Arndt, M. Ben Dahan, D. Guéry-Odelin, M. W. Reynolds, and J. Dalibard, *Phys. Rev. Lett.* **79**, 625 (1997).
- [12] D. Guéry-Odelin, J. Soeding, P. Desbiolles, and Jean Dalibard, *Opt. Express* **2**, 323 (1998).
- [13] H. Weichenmeier, U. Diemer, M. Wahl, M. Raab, W. Wüller, and W. Demtröder, *J. Chem. Phys.* **82**, 5354 (1985).
- [14] P. J. Leo, P. S. Julienne, F. H. Mies, and C. J. Williams, *Phys. Rev. Lett.* **86**, 3743 (2001).
- [15] P. J. Leo, C. J. Williams, and P. S. Julienne, *Phys. Rev. Lett.* **85**, 2721 (2000).
- [16] V. Vuletić, C. Chin, A. J. Kerman, and S. Chu, *Phys. Rev. Lett.* **83**, 943 (1999).
- [17] C. Chin, V. Vuletić, A. J. Kerman, and S. Chu, *Phys. Rev. Lett.* **85**, 2717 (2000).
- [18] V. Vuletić, A. J. Kerman, C. Chin, and S. Chu, *Phys. Rev. Lett.* **82**, 1406 (1999).
- [19] Ph. Courteille, R. S. Freeland, D. J. Heinzen, F. A. van Abeelen, and B. J. Verhaar, *Phys. Rev. Lett.* **81**, 69 (1998).
- [20] I. H. Deutsch and P. S. Jessen, *Phys. Rev. A* **57**, 1972 (1998).
- [21] V. Vuletić, C. Chin, A. J. Kerman, and S. Chu, *Phys. Rev. Lett.* **81**, 5768 (1998).
- [22] A. J. Kerman, V. Vuletić, C. Chin, and S. Chu, *Phys. Rev. Lett.* **84**, 439 (2000).
- [23] S. Friebe, C. D'Andrea, J. Walz, M. Weitz, and T. W. Hänsch, *Phys. Rev. A* **57**, R20 (1998).
- [24] D. J. Han, M. T. DePue, and D. S. Weiss, *Phys. Rev. A* **63**, 023405 (2001).
- [25] M. Arndt, M. Ben Dahan, D. Guery-Odelin, M. W. Reynolds, and J. Dalibard, *Phys. Rev. Lett.* **79**, 625 (1997).
- [26] J. Soding, D. Guery-Odelin, P. Desbiolles, G. Ferrari, and J. Dalibard, *Phys. Rev. Lett.* **80**, 1869 (1998).
- [27] D. Guery-Odelin, J. Soding, P. Desbiolles, and J. Dalibard, *Opt. Express* **2**, 323 (1998).
- [28] T. Weber, J. Herbig, M. Mark, H.-C. Nägerl, and R. Grimm, *Phys. Rev. Lett.* **91**, 123201 (2003).
- [29] J. L. Roberts, N. R. Claussen, James P. Burke, Jr., Chris H. Greene, E. A. Cornell, and C. E. Wieman, *Phys. Rev. Lett.* **81**, 5109 (1998).
- [30] N. F. Mott, and H. S. W. Massey, *The Theory of Atomic Collisions* (Clarendon Press, Oxford, 1965).
- [31] E. Arimondo, M. Inguscio, and P. Violino, *Rev. Mod. Phys.* **49**, 31 (1977).
- [32] R. G. Gordon, *J. Chem. Phys.* **51**, 14 (1969); *Methods Comput. Phys.* **10**, 81 (1971).
- [33] H. T. C. Stoof, J. M. V. A. Koelman, and B. J. Verhaar, *Phys. Rev. B* **38**, 4688 (1988).
- [34] D. T. Colbert and W. H. Miller, *J. Chem. Phys.* **96**, 1982 (1992); E. Tiesinga, C. J. Williams and P. S. Julienne, *Phys. Rev. A* **57**, 4257 (1998).
- [35] F. H. Mies and M. Raoult, *Phys. Rev. A* **62**, 012708 (2000).
- [36] J. M. Vogels, B. J. Verhaar, and R. H. Blok, *Phys. Rev. A* **57**, 4049 (1998).
- [37] T. Laue, E. Tiesinga, C. Samuelis, H. Knöckel, and E. Tiesmann, *Phys. Rev. A* **65**, 023412 (2002).
- [38] R. Napolitano, J. Weiner, C. J. Williams, and P. S. Julienne, *Phys. Rev. Lett.* **73**, 1352 (1994).
- [39] T. Weber, J. Herbig, M. Mark, H.-C. Nägerl, and R. Grimm, *Science* **299**, 232 (2003).